The 2010 IEEE/RSJ International Conference on
Intelligent Robots and Systems
October 18-22, 2010, Taipei, Taiwan

Compact self-contained navigation system with MEMS inertial sensor and optical navigation sensor for 3-D pipeline mapping

Dongjun Hyun, Minsu Jegal and Hyun Seok Yang

Abstract— **We propose a compact self-contained navigation system with Micro-Electro-Mechanical System (MEMS) inertial sensor and optical navigation sensor for 3-D pipeline mapping. Self-contained navigation system have advantages of robust against severe environmental conditions and also wide applications without external assist such as Global Positioning System (GPS) navigation or localization system based on a map. The goal of this study is to overcome the performance limitations of small, low-grade sensors by combining various sensors with complementary functions and, therefore, to achieve robust tracking performance against severe environmental conditions. The multi-rate EKF solves the frequent outage problem of the optical navigation sensors and the bias drift problem of the MEMS accelerometers. The vector matching algorithm with the gravity field vector solves the bias drift problem of the MEMS gyro except for the yaw in the reference axis. The geometry compensation algorithm minimizes position errors by combining the forward and backward estimation results geometrically. Experiments to verify performance are conducted by driving Radio-Controlled (RC) car equipped with the proposed navigation system on 3-D asphalt pavement. Experimental results show that the proposed navigation system has good performance and estimated position errors are less than one percent, in the range of 855 m. The proposed navigation system can contribute a compact size and robustness not only to 3-D pipeline mapping but also to small mobile robots.**

I. INTRODUCTION

3-D pipeline mapping is important for the inspection and repair of most pipelines. For pipelines buried under cities where incessant construction increases the confusion of pipeline positioning, the need for 3-D mapping significantly increases in order to prevent the damage of pipelines from works such as excavation and construction. Tap water pipelines have several difficulties using 3-D pipeline mapping with established methods such as a geometry pig used in gas/oil industries or ground penetrating radar (GPR). A geometry pig equipped with a precise inertial measurement unit and wheel type odometer is not suitable for most tap water pipelines because the diameter of most tap water pipelines is much smaller than that of gas/oil industries and the pipe scales of tap water pipelines disturb the odometer. Complex underground conditions and obstacles, such as buildings and walls, disturb and confuse the GPR.

The sensor system and tracking algorithm proposed in this study are designed to achieve acceptable performance, size reduction and robustness against severe environments by applying an adequate sensor fusion algorithm and constructing a sensor system that consists of sensors with complementary function, although the individual performance of sensors are low.

The self-contained sensor system consists of a small, low-cost MEMS inertial sensor and an optical navigation sensor, which is recently substituted with an odometer in [1]-[4] but is fused with the MEMS IMU to overcome the weakness of the optical navigation sensor. A small, low-cost MEMS IMU is conventionally used with wheel-type odometers, GPS, or a vision system, due to the bias drift [5]-[9]. Optical navigation sensors typically used in mice measure displacement with a noncontact-type sensor by comparing surface images of the current and previous frame and, unlike wheel-type odometers, are free from slip. Optical navigation sensors sometimes fail to measure the displacement, but this failure should be distinguished from the slipping of the wheel-type odometers, since detecting the failure of the optical navigation sensors is much easier than slip error detection.

The tracking algorithm consists of a multi-rate EKF to estimate the states of the nonlinear system with redundant sensors that have different sampling rates, a vector matching algorithm to guarantee bounded roll and pitch errors in reference axes and a geometry compensation method to minimize the position error of the estimated path by combining the two geometry curves obtained by forward and backward estimation. Multi-rate EKF fuses the inertial and optical navigation sensor measurements using multi-rate sampling that is necessary to treat asynchronous sensor data and irregularly occurring optical navigation sensor failures. The position error reduction method using the start and the end points in pipeline mapping was developed by backward smoothing filter in [6] and [10]. In this paper, the geometric approach is applied to address the same problem.

II. COMPACT SELF-CONTAINED SENSOR SYSTEM

A. Overview of Compact Sensor System

The sensor system consists of a MEMS inertial sensor, a couple of optical navigation sensors, a central processing unit (CPU), and a secure digital (SD) card. The CPU module in

Dongjun Hyun is with the Department of Mechanical Engineering, Yonsei University, 262, Seongsanno, Seodamun-gu, Seoul, 120-749, Korea (e-mail: dongjunn@yonsei.ac.kr).

Minsu Jegal is with the Department of Mechanical Engineering, Yonsei University, 262, Seongsanno, Seodamun-gu, Seoul, 120-749, Korea (e-mail: jglupin@yonsei.ac.kr).

Hyun Seok Yang is with the Department of Mechanical Engineering, Yonsei University, 262, Seongsanno, Seodamun-gu, Seoul, 120-749, Korea (corresponding author to provide phone: 82-2-2123-2824; fax: 82-2-364-6769; e-mail: hsyang@yonsei.ac.kr).

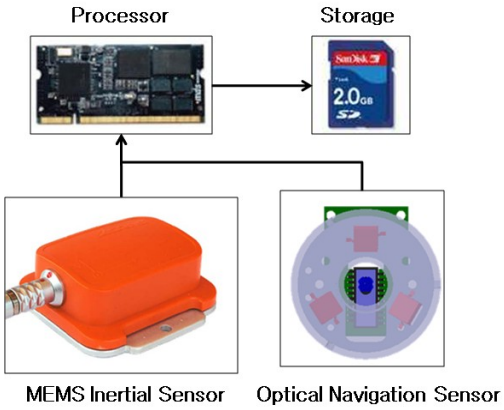

Fig. 1. Overview of the compact system.

this study is comprised of an S3C2440 processor using an ARM920T core, 4MByte Nor Flash, 64MByte Nand Flash, and 64MByte SDRAM. The CPU module stored the SD card with the MEMS inertial sensor and optical navigation sensor measurements for the post-processing of the experimental data. The MEMS inertial sensor is interfaced with an RS-232 and had a sampling period of 10 msec. The optical navigation sensor is interfaced with the serial peripheral interface (SPI) and provided a sampling period of 5 msec or less. The dimensions of the MEMS inertial sensor is 58x58x22 mm, and the optical navigation sensor is 55x55x31 mm. Figure 1 shows the overview of the compact sensor system.

B. MEMS Inertial Sensor

An Xsens MTi, a small, low-cost MEMS inertial measurement unit (IMU), is used as an inertial sensor and have a sensing range of ±300°/sec (angular rate) and ±2g (acceleration).

C. Optical Navigation Sensor

An Avago Technologies ADNS6010 optical navigation sensor is usually applied to laser computer mice and is comprised of a 30x30 pixel image sensor and a digital signal processor (DSP) for image processing. An optical navigation sensor can be applied as an odometer and benefits from the fact that noncontact-type measurements do not experience the slip ambiguity that plagues wheel-type odometers. Although an optical navigation sensor occasionally fails to process the surface image, the outage from an optical navigation sensor can be clearly detected and treated more easily than the slip error from the estimation algorithm. For the laser mice, the optical system is comprised of a lens and a laser diode illumination source, and functions only when the optical navigation sensor is 2-3mm from the surface. Therefore, application for rough surface, a new optical system comprised of a micro lens and LEDs is designed so that an optical navigation sensor is usable even when the optical navigation sensor is located 20-80mm away from the surface. Figure 2 shows the newly designed optical system.

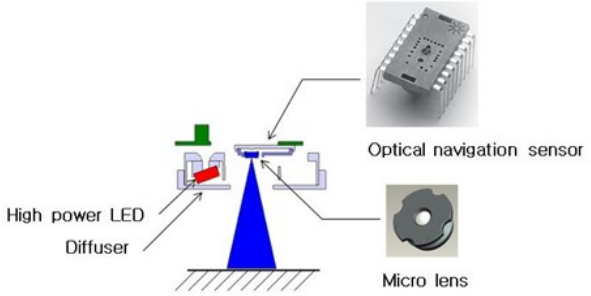

Fig. 2. An optical navigation sensor and the new optical system.

III. NAVIGATION ALGORITHM

A. Multi-rate EKF Algorithm

Despite several shortcomings, the EKF is the most popular recursive state estimator for a nonlinear system. The multi-rate sampling method was applied to EKF for an asynchronous sensor system consisting of sensors with different sampling rates in [5]. Multi-rate EKF is most suitable for the sensor system proposed in this paper because the MEMS IMU and optical navigation sensor have different sampling rates and the outage of the optical navigation sensor is irregular. Table 1 shows the process of a multi-rate EKF, consisting of the measurement, prediction and Kalman filtering steps. Where $\mathbf{z}_{k+1}$, $\mathbf{H}_{k+1}$ and $\mathbf{r}_{k+1}$ denote a measurement vector sampled at the k+1 step, a measurement model matrix, a diagonal vector of the measurement noise covariance matrix $\mathbf{R}_{k+1}$ respectively, and $\mathbf{x}_k$ denote a state vector at the k step. $\mathbf{P}_{k+1}$, $\mathbf{F}_{k+1}$, $\mathbf{Q}_{k+1}$ and $\mathbf{K}_{k+1}$ denote a covariance matrix of the state vector, a state propagation matrix, a covariance matrix of the process noise $\mathbf{w}_{k+1}$ and a Kalman gain matrix, respectively.

TABLE I
PROCESS OF THE MULTI-RATE EKF

Process	Multi-rate EKF
Measurement	$\mathbf{z}_{k+1} = [\ ]^T$, $\mathbf{H}_{k+1} = [\ ]$ and $\vec{\mathbf{r}}_{k+1} = \lfloor\ \rfloor$ if $\mathbf{z}_{1,k+1}, \mathbf{z}_{k+1} = \left[\mathbf{z}^T \quad \mathbf{z}_1^T\right]_{k+1}^T$, $\mathbf{H}_{k+1} = \left[\mathbf{H}^T \quad \mathbf{H}_{z1}^T\right]_{k+1}^T$ and $\vec{\mathbf{r}}_{k+1} = \lfloor \vec{\mathbf{r}} \quad \vec{\mathbf{r}}_{z1} \rfloor_{k+1}$ if $\mathbf{z}_{2,k+1}, \mathbf{z}_{k+1} = \left[\mathbf{z}^T \quad \mathbf{z}_2^T\right]_{k+1}^T$, $\mathbf{H}_{k+1} = \left[\mathbf{H}^T \quad \mathbf{H}_{z2}^T\right]_{k+1}^T$ and $\vec{\mathbf{r}}_{k+1} = \lfloor \vec{\mathbf{r}} \quad \vec{\mathbf{r}}_{z2} \rfloor_{k+1}$ ⋮
Prediction	$\bar{\mathbf{x}}_{k+1} = f\left(\mathbf{x}_k, \mathbf{u}_{k+1}, \mathbf{w}_{k+1}\right)$ $\bar{\mathbf{P}}_{k+1} = \mathbf{F}_{k+1}\mathbf{P}_k\mathbf{F}_{k+1}^T + \mathbf{Q}_{k+1}$
Kalman filtering	if $\mathbf{z}_{k+1}$, $\mathbf{R}_{k+1} = diag\left(\vec{\mathbf{r}}_{k+1}\right)$ $\mathbf{K}_{k+1} = \bar{\mathbf{P}}_{k+1}\mathbf{H}_{k+1}^T\left(\mathbf{H}_{k+1}\bar{\mathbf{P}}_{k+1}\mathbf{H}_{k+1}^T + \mathbf{R}_{k+1}\right)^{-1}$ $\mathbf{x}_{k+1} = \bar{\mathbf{x}}_{k+1} + \mathbf{K}_{k+1}\left(\mathbf{z}_{k+1} - \mathbf{H}_{k+1}\bar{\mathbf{x}}_{k+1}\right)$ $\mathbf{P}_{k+1} = \left(\mathbf{I} - \mathbf{K}_{k+1}\mathbf{H}_{k+1}\right)\bar{\mathbf{P}}_{k+1}$ else $\mathbf{x}_{k+1} = \bar{\mathbf{x}}_{k+1}$ $\mathbf{P}_{k+1} = \bar{\mathbf{P}}_{k+1}$

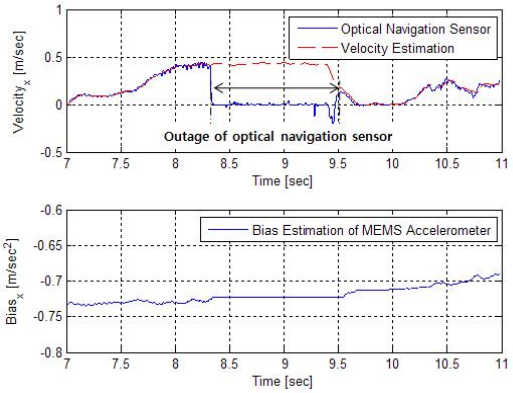

Fig. 3. Results of the velocity and accelerometer bias estimations.

During irregular and temporary outages of the optical navigation sensors, we estimated the velocity vector with only the MEMS accelerometers since the bias vector of the MEMS accelerometers changes sufficiently slowly, within a few seconds. As part of the EKF process, we assigned very small values to the process noise matrix corresponding to the state vector of the biases for the purpose of suppressing the state vector change. Figure 3 shows that we were able to estimate the velocity continuously and successfully during a short outage of the optical navigation sensor and that the bias changed slowly and very little during the short outage.

B. Vector Matching Algorithm

The vector matching algorithm is the attitude-determination algorithm based on the two non-collinear, non-zero vector measurements that present the magnetic field vector from the triad magnetometer and the gravity vector from the triad accelerometer in [11] and [12]. The vector matching algorithm guarantees bounded attitude errors with small, low-cost sensors since both the magnetic and gravity field vectors give absolute attitude information within the frame of the Earth. However, the triad magnetometer is not suitable for small mobile robots since the permanent magnets and varying currents within motors of the small mobile robot interrupt to find the magnetic field vector of the Earth.

We modified the vector matching algorithm in order to determine attitude from the gravity field vector and the rate-gyro. The roll and pitch of the Earth frame are determined by the gravity field vector, and the yaw is determined by the triad rate gyro. In order to suppress the biases of small, low-cost gyros to disturb attitude estimations, biases were estimated during every stop state of the mobile robot.

The attitude estimation was implemented as follows:

1) Compute the estimated attitude $\hat{\mathbf{q}}_{k+1}$ by propagating $\mathbf{q}_k$ with the sampled rate gyros.

2) Estimate the attitude error quaternion vector $\vec{\mathbf{q}}_{e,k+1}$ using the vector matching algorithm. Where $\vec{\mathbf{q}}_e$ is (1).

$$\vec{\mathbf{q}}_e = \lfloor q_{e1} \quad q_{e2} \quad q_{e3} \rfloor^T \tag{1}$$

3) Compute the true attitude quaternion $\mathbf{q}_{k+1}$ using the following:

$$\mathbf{q}_{k+1} = \hat{\mathbf{q}}_{k+1} \otimes \mathbf{q}_{e,k+1}$$

$$= \mathbf{Q}'_{e,k+1} \hat{\mathbf{q}}_{k+1} \tag{2}$$

$$\mathbf{Q}'_{e,k+1} = \begin{bmatrix} 1 & 0 & 0 & 0 \\ q_{e1} & 1 & -q_{e3} & q_{e2} \\ q_{e2} & q_{e3} & 1 & -q_{e1} \\ 0 & 0 & 0 & 1 \end{bmatrix} \tag{3}$$

We modified $\mathbf{Q}'_{e,k+1}$ to prevent $\vec{\mathbf{q}}_{e,k+1}$ from disturbing the yaw by setting first and forth rows identities.

4) Normalize the true attitude quaternion $\mathbf{q}_{k+1}$ using the following:

$$\mathbf{q}_{k+1} = \frac{\mathbf{q}_{k+1}}{\|\mathbf{q}_{k+1}\|} \tag{4}$$

C. Geometry Compensation Algorithm

The geometry compensation algorithm proposed in this paper represents a method to reduce error in the position estimation by combining the two curves obtained from the forward and backward estimations with a geometric approaching method. For the 3-D pipeline mapping, for which start and end points are given, the maximum position error of the method using both forward and backward estimations can be less than half of the method using only forward estimation or backward estimation because the position error of dead reckoning navigation increases exponentially over time and distance.

The geometry compensation algorithm is implemented as follows.

1) Obtain the geometric curve from the forward estimations.

2) Obtain the geometric curve from the backward estimations.

3) Find a couple of closest points on the two curves respectively and the middle point between the two points.

4) Select $\mathbf{p_0}$, $\mathbf{p_1}$ and $\mathbf{p_2}$. $\mathbf{p_0}$ and $\mathbf{p_2}$ lies on the two estimation curve respectively and are adequate distant from the closest points. $\mathbf{p_1}$ is the middle point between the two closes points.

5) Construct the quadratic Bezier curve with $\mathbf{p_0}$, $\mathbf{p_1}$ and $\mathbf{p_2}$ using the following:

$$\mathbf{p}_{Bezier}(t) = (1-t)^2 \mathbf{p}_0 + 2(1-t)t\mathbf{p}_1 + t^2\mathbf{p}_2, \; t \in [0,1] \tag{5}$$

6) Construct the geometric compensation curve as the following:

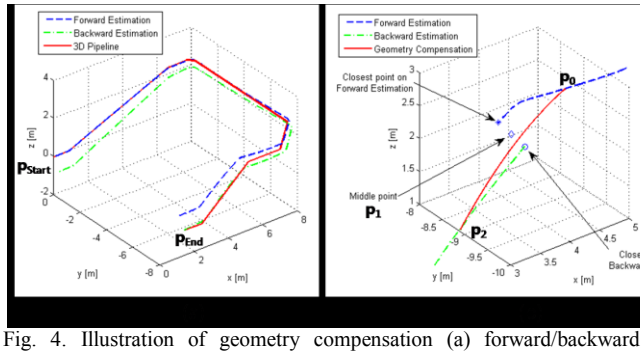

Fig. 4. Illustration of geometry compensation (a) forward/backward estimation curves (b) geometry compensation procedure.

$$\mathbf{p}^{n} = \begin{cases} \mathbf{p}_{\text{Forward Estimation}} & [\mathbf{p}_{\text{Start}},\ \mathbf{p}_{0}] \\ \mathbf{p}_{\text{Bezer}} & [\mathbf{p}_{0},\ \mathbf{p}_{2}] \\ \mathbf{p}_{\text{Backward Estimation}} & [\mathbf{p}_{2},\ \mathbf{p}_{\text{End}}] \end{cases} \tag{6}$$

Figure 4 shows the illustration of the geometry compensation algorithm.

D. Implementation of Navigation Algorithms

The discrete model of states and measurements of this paper is given by (7)-(26) based on [5], [11] and [12].

$$\mathbf{x}_{k+1} = f(\mathbf{x}_k, \mathbf{w}_k) \tag{7}$$

$$\mathbf{x}_k = \left[\mathbf{p}^T \quad \mathbf{v}^T \quad \mathbf{a}^T \quad \mathbf{b}^T \quad \boldsymbol{\omega}^T \quad \vec{\mathbf{q}}_e^{\,T}\right]_k \tag{8}$$

$$\mathbf{w}_k = \left[\mathbf{j}^T \quad \mathbf{b}'^T \quad \boldsymbol{\alpha}^T \quad \vec{\mathbf{q}}_e^{\,T}\right]_k \tag{9}$$

$$\mathbf{a}' = \mathbf{j} + \boldsymbol{\alpha} \times \mathbf{v} + \boldsymbol{\omega} \times \mathbf{a} \tag{10}$$

$$\mathbf{p}_{k+1} = \mathbf{p}_k + T \cdot \mathbf{v}_k + \frac{T^2}{2} \cdot \mathbf{a}_k + \frac{T^3}{6} \cdot \mathbf{a}'_k \tag{11}$$

$$\mathbf{v}_{k+1} = \mathbf{v}_k + T \cdot \mathbf{a}_k + \frac{T^2}{2} \cdot \mathbf{a}'_k \tag{12}$$

$$\begin{aligned} \mathbf{a}_{k+1} &= \mathbf{a}_k + T \cdot \mathbf{a}'_k \\ &= \mathbf{a}_k + T \cdot \left(\mathbf{j}_k + \boldsymbol{\alpha}_k \times \mathbf{v}_k + \boldsymbol{\omega}_k \times \mathbf{a}_k\right) \end{aligned} \tag{13}$$

$$\mathbf{b}_{k+1} = \mathbf{b}_k + T \cdot \mathbf{b}'_k \tag{14}$$

$$\boldsymbol{\omega}_{k+1} = \boldsymbol{\omega}_k + T \cdot \boldsymbol{\alpha}_k \tag{15}$$

$$(\vec{\mathbf{q}}_e)_{k+1} = (\mathbf{I} + T \cdot \boldsymbol{\omega}_k) \times (\vec{\mathbf{q}}_e)_k + T \cdot (\vec{\mathbf{q}}_e)_k \tag{16}$$

$$\mathbf{z}_{k+1} = \mathbf{H}_{k+1}\mathbf{x}_{k+1} + \mathbf{v}_{k+1} \tag{17}$$

$$\begin{aligned} \mathbf{z}_{k+1} &= \left[\mathbf{z}_1^T \quad \mathbf{z}_2^T \quad \mathbf{z}_3^T \quad \mathbf{z}_4^T\right]_{k+1}^T \\ &= \left[\mathbf{a}_{Inertial}^T \quad \mathbf{g}_{Inertial}^T \quad \boldsymbol{\omega}_{Inertial}^T \quad \mathbf{p}_{Optical}^T\right]_{k+1}^T \end{aligned} \tag{18}$$

$$\mathbf{v}_{k+1} = \left[\mathbf{v}_{\mathbf{a}_{Inertial}}^T \quad \mathbf{v}_{\mathbf{g}_{Inertial}}^T \quad \mathbf{v}_{\boldsymbol{\omega}_{Inertial}}^T \quad \mathbf{v}_{\mathbf{p}_{Optical}}^T\right]_{k+1}^T \tag{19}$$

$$\begin{aligned} \mathbf{a}_{Inertial} &= \mathbf{a}_{raw} - \mathbf{Q}_n^b \mathbf{g}^n \\ &= \mathbf{a} + \mathbf{b} \end{aligned} \tag{20}$$

$$\begin{aligned} \mathbf{g}_{Inertial} &= \mathbf{Q}_b^n \left(\mathbf{a}_{raw} - \mathbf{a} - \boldsymbol{\omega} \times \mathbf{v} - \mathbf{b}\right) \\ &= -2\mathbf{g}^n \times \vec{\mathbf{q}}_e \end{aligned} \tag{21}$$

$$\boldsymbol{\omega}_{Inertial} = \boldsymbol{\omega} \tag{22}$$

$$\mathbf{p}_{Optical} = \mathbf{p}_{k+1} + T \cdot \mathbf{v}_{k+1} + \frac{T^2}{2}\mathbf{a}_{k+1} \tag{23}$$

$$\Delta\mathbf{p}_{k+1}^b = \mathbf{p}_{k+1} - \mathbf{p}_k \tag{24}$$

$$\Delta\mathbf{p}_{k+1}^n = \mathbf{Q}_b^n \Delta\mathbf{p}_{k+1}^b \tag{25}$$

$$\mathbf{p}_{k+1}^n = \mathbf{p}_k^n + \Delta\mathbf{p}_{k+1}^n \tag{26}$$

IV. Experimental Results

A. Experimental Equipments and Reference Path

The compact navigation system was tested with an RC car on the reference path measured with D-GPS. The RC car of which the size was 370x260x140 mm was a common 1/10th scale electric touring car and was equipped with tires of RC trucks. The sensor system was simply attached to the RC car as shown on figure 5 and was compact enough to be installed to the RC car without any bulky unbalance.

The reference path was asphalt pavement in the Wabu filtration plant and was precisely measured with D-GPS before the experiment. The total distance of the reference path was 855.4m and the reference path had 3-dimensional shape with height variation of approximately 5.5 m. Figure 6 shows the measured reference path overlapped with the aerial photography of the Wabu filtration plant.

We drove the RC car equipped with the sensor system at the speed of approximately 3 m/s along the reference path as coincidently as possible.

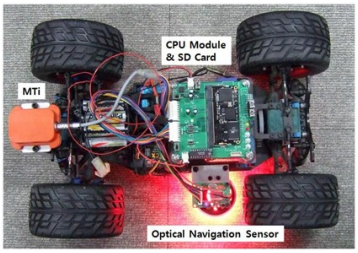

Fig.5. Self-contained navigation system on an RC car.


Fig. 6. Asphalt pavement measurements in the Wabu filtration plant.

B. Estimation Results

Figures 7 (a) and (b) represent the position estimation results using the proposed navigation algorithms with both forward and backward directions. The position error increased rapidly for the yaw-directional component of the attitude estimation as the RC car passed through the corner approximately 500 m from the starting point. The other directional components such as roll, pitch and linear displacement showed little error.

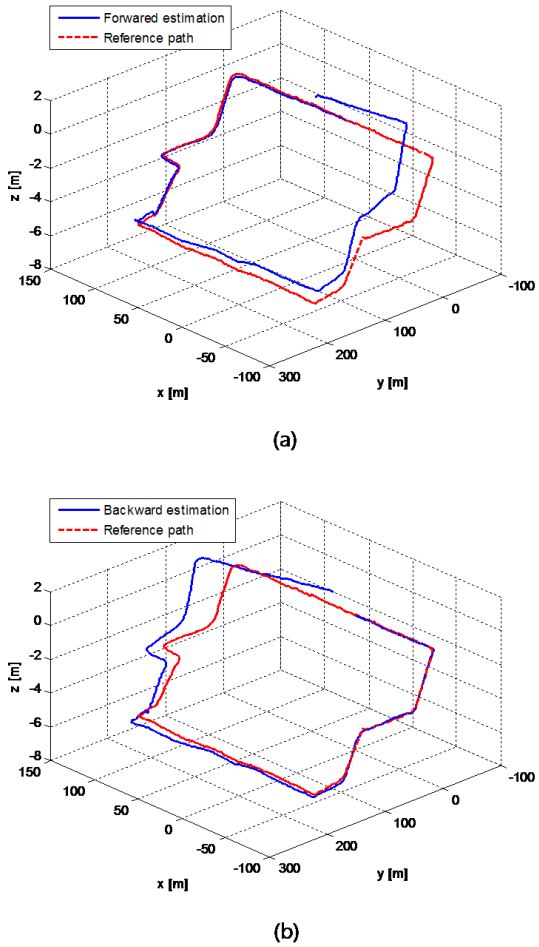

Fig. 7. Results of (a) forward estimation and (b) backward estimation.

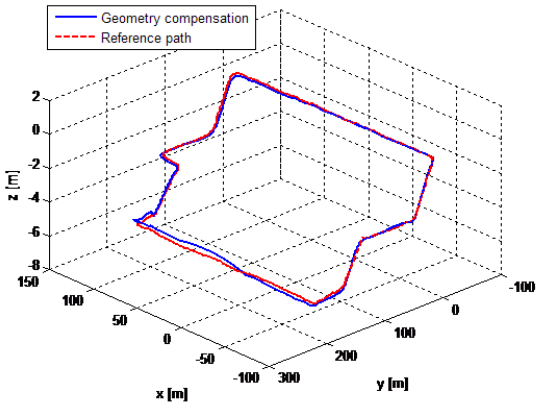

Fig. 8. Result path of the geometry compensation algorithm.

The result path of the geometry compensation algorithm shown on figure 8 is coincident with the reference path well. Figures 9 (a) and (b) shows the position error of the estimated path as a minimum distance between the reference points of the asphalt pavement and the estimated path. Position errors of both forward estimation and backward estimation have the same pattern that errors start increasing rapidly from the middle stage. The position error is proportional to the distance between forward estimation and backward estimation since the closest point locates on the straight region of the path. Therefore, the junction point on figure 9 (a) means the closest point of the geometry compensation algorithm. The maximum position error of the geometry compensation algorithm is less than 2.5 m with a total distance 855.4 m.

Velocity estimation is successful although many intermittent outages of the optical navigation sensor happen during the test as shown on figure 10. Figures 11 (a) and (b) show proper estimating processes with the multi-rate EKF algorithm during outages of the optical navigation sensor clearly. If the algorithm detects the outage of the optical navigation sensor, then the algorithm excludes data of the optical navigation sensor and processes velocity estimation with estimated accelerations and biases.

Figures 12 (a) and (b) show estimated states of velocity and quaternion. The q_3-directional component in the attitude quaternion represents yawing motion and the q_1-directional and q_2-directional components represent the rolling and pitching motion. The rolling and pitching components keep stable states due to the vector matching algorithm.

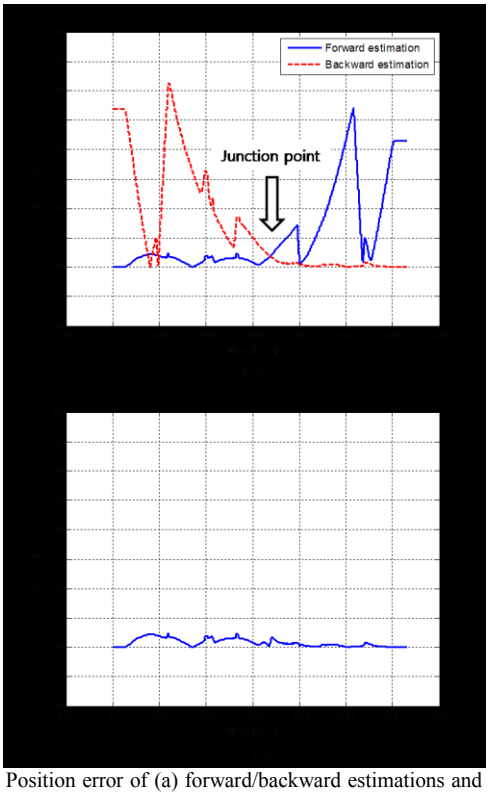

Fig. 9. Position error of (a) forward/backward estimations and (b) the geometry compensation algorithm.

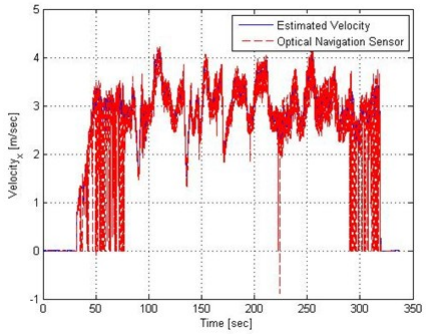

Fig. 10. Estimated velocity and optical navigation sensor.

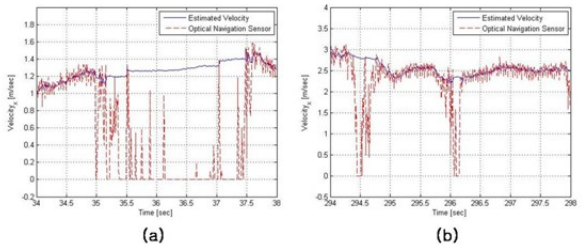

Fig. 11. Estimated velocity and optical navigation sensor at (a) 34-38 sec and (b) 294-289 sec.

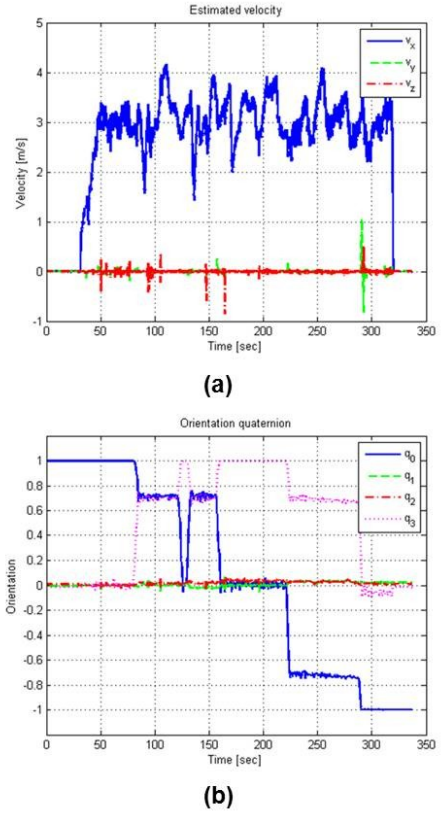

Fig. 12. Estimated states of (a) velocity and (b) quaternion

V. Conclusions and Future Works

These experimental results have demonstrated that the self-contained navigation system, including the optical navigation sensor developed for this study, functions successfully and can successfully estimate the path of a RC car. In particular, the navigation algorithms have combined redundant and complementary measurements of the optical navigation sensor and the low cost MEMS inertial sensors, as well as successfully restoring the displacement of the optical navigation sensor measurements. Although only the gravity field vector was used, the modified vector matching algorithm functions successfully.

Future research will aim to combine the self-contained navigation system with a simultaneous localization and mapping (SLAM) system. Fusion of the self-contained navigation and the SLAM system is expected to eliminate the weakness of the individual systems since the self-contained navigation system provides the SLAM system with both accurate and fast motion information and the SLAM system provides a self-contained navigation system with bounded-error pose information.

References

[1] Cooney J.A., Xu W.L. and Bright G., "Visual dead-reckoning for motion control of a Mecanum-wheeled mobile robot," Mechatronics, 14, 623-637, 2004.

[2] Lee, S. and Song, J. B., "Robust Mobile Robot Localization using Optical Flow Sensors and Encoders," International Conference on Robotics and Automation (ICRA), 1039-1044, 2004.

[3] Bonarini, A., Matteucci, M. and Restelli, M., "Automatic Error Detection and Reduction for an Odometric Sensor based on Two Optical Mice," IEEE International Conference on Robotics and Automation (ICRA), 1675-1680, 2005.

[4] Tunwattana, N., Roskilly, A. P. and Norman, R., "Investigations into the effects of illumination and acceleration on optical mouse sensors as contact-free 2D measurement devices," Sensors and Actuators A:Physical, 149, 87-92, 2009.

[5] Armesto, L., Tornero, J. and Vincze, M., "Fast Ego-motion Estimation with Multi-rate Fusion of Inertial and Vision," International Journal of Robotics Research, 26(6), 577-589, 2007.

[6] Yu J, Lee JG, Park CG and Han HS, "An off-line navigation of a geometry PIG using a modified nonlinear fixed-interval smoothing filter", Control Engineering Practice, 13, 1403-1411, 2005.

[7] Bavly, D. M., Parkinson, B., "Cascaded Kalman Filters for Accurate Estimation of Multiple Biases, Dead-Reckoning Navigation, and Full State Feedback Control of Ground Vehicles", IEEE Transactions on Control Systems Technology, 15(2), 199-208, 2007.

[8] López-Orozco, J. A., de la Cruz, J. M., Besada, E. and Ruipérez, P., "An Asynchronous, Robust, and Distributed Multisensor Fusion System for Mobile Robots", International Journal of Robotics Research, 19(10), 914-932, 2000.

[9] Sukkarieh, S., Nebot, E.M. and Durrant-Whyte, H.F, "A high integrity IMU/GPS navigation loop for autonomous land vehicle applications", IEEE Transactions on Robotics and Automation, 15(3), 572 – 578, 1999.

[10] Nassar, S., "Improving the Inertial Navigation System (INS) Error Model for INS and INS/DGPS Applications", PhD Thesis, Department of Geomatics Engineering, University of Calgary, Calgary, Alberta, Canada, UCGE Report No. 20183, 2003.

[11] Gebre-Egziabher, D., Hayward, R. C. and Powell, J. D., "Design of Multi-Sensor Attitude Determination Systems," IEEE Transactions on Aerospace and Electronic Systems, 40(2), 627-649, 2004.

[12] Gebre-Egziabher, D. and Elkaim, G. H., "MAV Attitude Determination by Vector Matching," IEEE Transactions on Aerospace and Electronic Systems, 44(3), 1012-1028, 2008.